CHAPTER IV
RESULTS AND DISCUSSION

4.1 Photocatalyst Characterizations

4.1.1 TG-DTA Results

The TG-DTA curves were used to study the thermal decomposition behavior of the synthesized dried TiO_2 photocatalyst and to obtain its suitable calcination temperature. Figure 4.1 shows the TG-DTA curves of the dried TiO_2 (a) without and (b) with 0.6 wt.% Pt loading by the SSSG method, which displayed the highest photocatalytic activity in a previous study (Sreethawong and Yoshikawa, 2006). The comparable total weight losses measured from the TG curves were 37.5 and 35.0 wt.% for unloaded and loaded photocatalysts, respectively. The DTA curves show three main exothermic regions. The details of the position of the exothermic peaks and their corresponding weight loss are summarized in Table 4.1. The first exothermic peak, with its position lower than 150°C, is attributed to the removal of physisorbed water molecules. The second exothermic peak between 150 and 300°C is very sharp and narrow and is attributed to the burnout of the surfactant template. The third exothermic region between 300 and 500°C consists of two weaker peaks that correspond to the crystallization process of the photocatalyst and also the elimination of organic remnants and chemisorbed water. The distinct difference of the thermal decomposition behavior of the dried Pt-loaded TiO_2 gel from the unloaded one is the intensity of the two exothermic peaks between 300 and 500°C in the DTA curves. However, there is insignificant weight loss observed from TG curves of both dried unloaded and Pt-loaded TiO_2 gels beyond the calcination temperature of 500°C. Therefore, the results confirm that the calcination temperature of 500°C was adequate for both complete surfactant template removal and photocatalyst crystallization process.

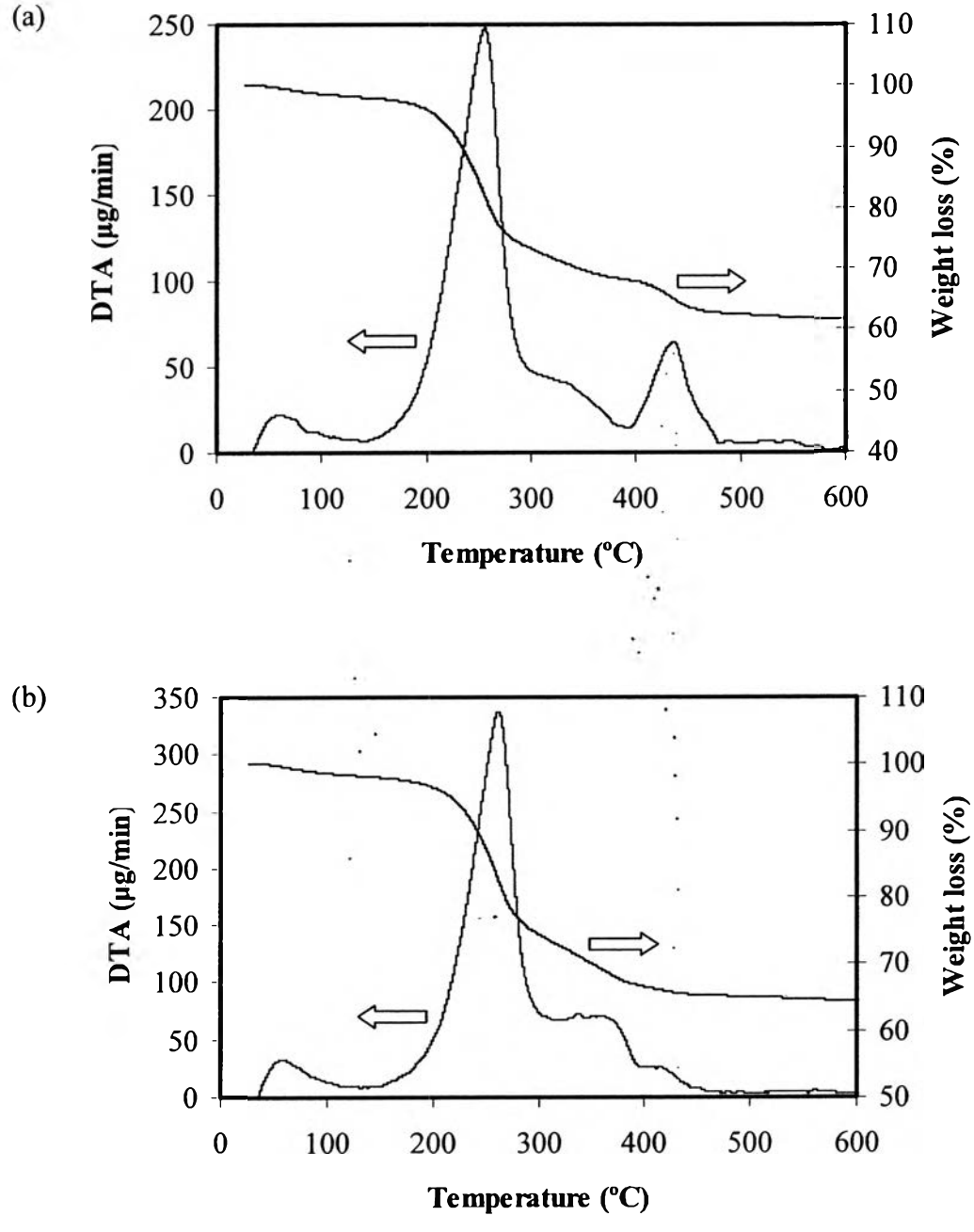

Figure 4.1 TG-DTA curves of (a) dried mesoporous-assembled TiO_2 and (b) dried 0.6 wt.% Pt- loaded mesoporous-assembled TiO_2 photocatalysts.

Table 4.1 Thermal decomposition behavior of the dried mesoporous-assembled TiO_2 and dried 0.6 wt.% Pt-loaded mesoporous-assembled TiO_2 photocatalysts from TG-DTA analysis

Photocatalyst	Position of exothermic peak (°C)				Corresponding weight loss (wt.%)				
	1st peak	2nd peak	3rd peak	4th peak	1st peak	2nd peak	3rd peak	4th peak	Total
Mesoporous-assembled TiO_2	61.6	255.3	334.0	435.1	2.1	24.7	5.4	5.3	37.5
0.6 wt.% Pt-loaded mesoporous-assembled TiO_2	58.3	260.4	366.0	420.2	2.0	23.6	7.9	1.5	35.0

4.1.2 N_2 Adsorption-Desorption Results

The N_2 adsorption-desorption analysis was used to verify the mesoporosity of the studied photocatalysts. The shape of the isotherms exhibits the characteristic behavior of the structure of powder, which is composed of an assembly of particles with large open packing. The adsorption-desorption isotherms of the unloaded mesoporous-assembled TiO_2 and 0.6 wt.% Pt-loaded mesoporous-assembled TiO_2 nanocrystals prepared by the SSSG method calcined at 500°C for 4 h are shown in Figures 4.2 and 4.3, respectively. They exhibit typical IUPAC type IV pattern with H2 hysteresis loop, which is the characteristic of mesoporous-assembled material (mesoporous size between 2-50 nm) according to the classification of IUPAC (Rouquerol *et al.*, 1999). A sharp increase in adsorption volume of N_2 was observed and located in the P/P_0 range of 0.5-0.9. This sharp increase can be attributed to the capillary condensation of N_2 inside the mesopores, indicating the good homogeneity of the sample and fairly small pore size since the P/P_0 position of the inflection point is directly related to the pore dimension. The inset of Figures 4.2 and 4.3 shows pore size distribution curve calculated from the desorption branch of

the isotherms by the BJH method. The samples possess monomodal and very narrow pore size distribution, identifying good quality of the samples.

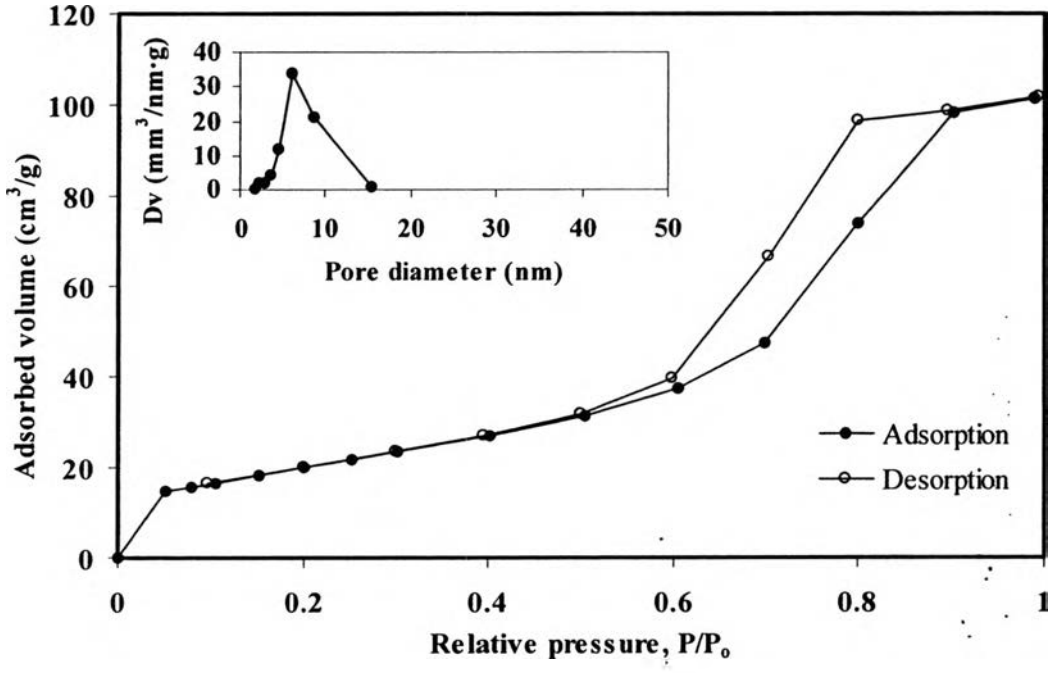

Figure 4.2 N_2 adsorption-desorption isotherms of the synthesized mesoporous-assembled TiO_2 calcined at 500°C for 4 h (Inset: pore size distribution).

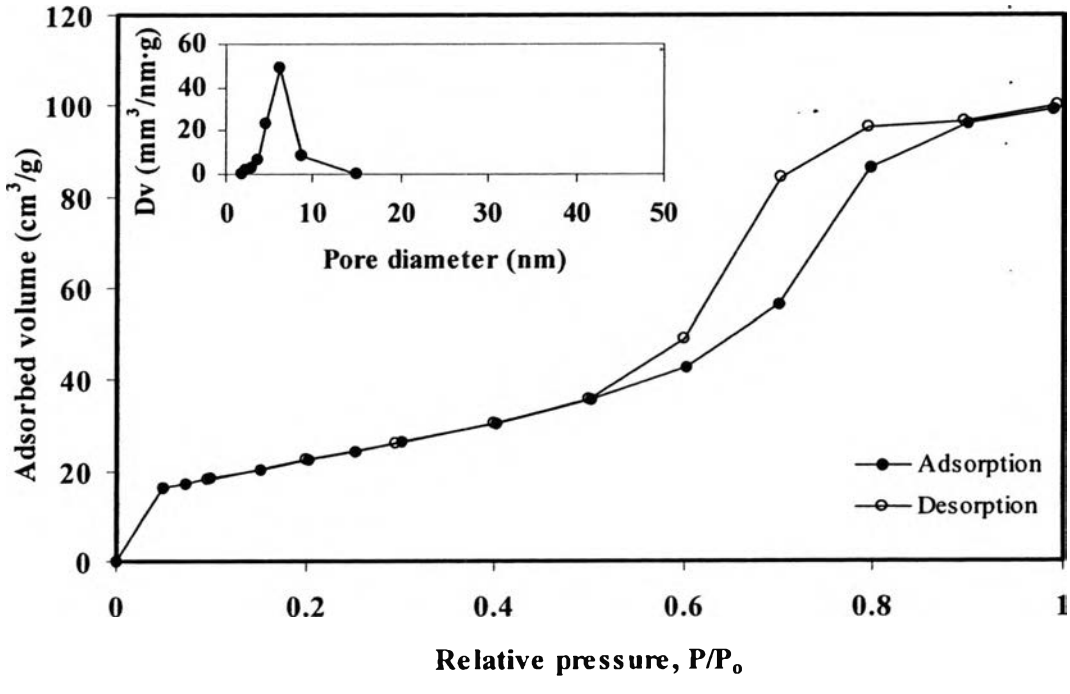

Figure 4.3 N_2 adsorption-desorption isotherms of the 0.6 wt.% Pt-loaded mesoporous -assembled TiO_2 calcined at 500°C for 4 h. (Inset: pore size distribution).

For the commercial P-25 TiO_2, ST-01 TiO_2, JRC-01 TiO_2, and JRC-03 TiO_2, N_2 adsorption-desorption isotherms of all commercial photocatalysts correspond to IUPAC type II pattern (Rouquerol *et al.*, 1999), as shown in Figures 4.4 to 4.7, respectively. It can be seen that all commercial TiO_2 photocatalysts possess non-mesoporous characteristic due to the absence of both distinct hysteresis loop and adsorption plateau at very high relative pressure, indicating no capillary condensation of N_2 into the pores. The pore size distributions of all commercial TiO_2 photocatalysts, as shown in the inset of Figures 4.4 to 4.7, are quite broad. These results show that the average pore size of the commercial P-25 TiO_2, ST-01 TiO_2, JRC-01 TiO_2, and JRC-03 TiO_2, are quite spacious because their pore size distributions are not only present in the mesoporous region (mesoporous size between 2-50 nm) but also mostly exist in the macroporous region (pore diameter > 50 nm).

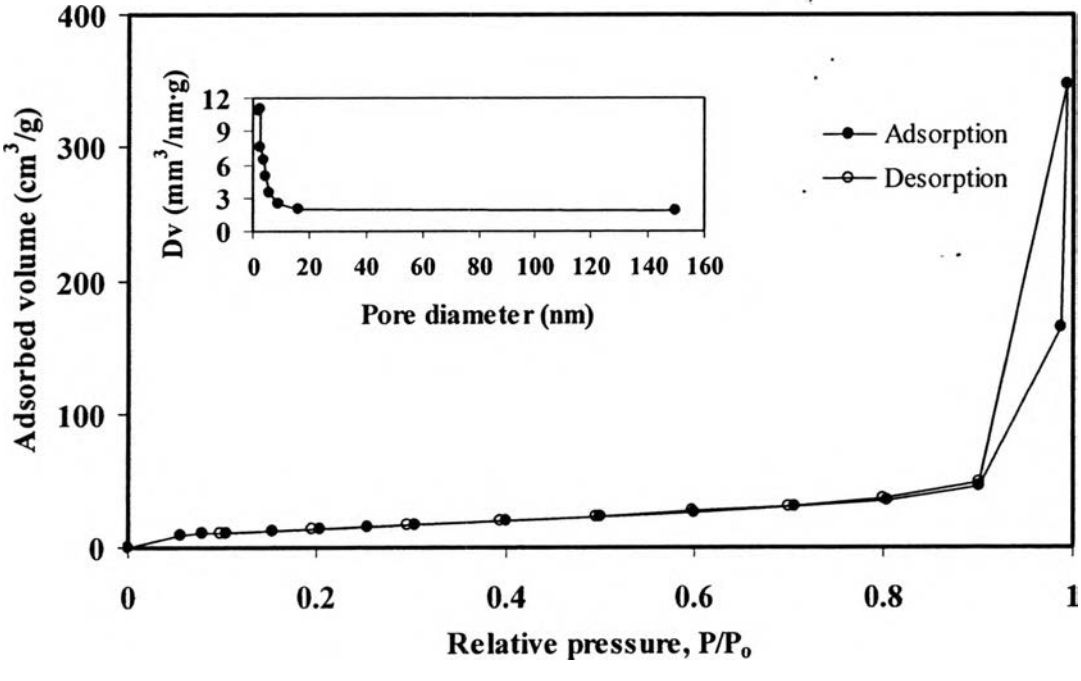

Figure 4.4 N_2 adsorption-desorption isotherms of the commercial P-25 TiO_2 (Inset: pore size distribution).

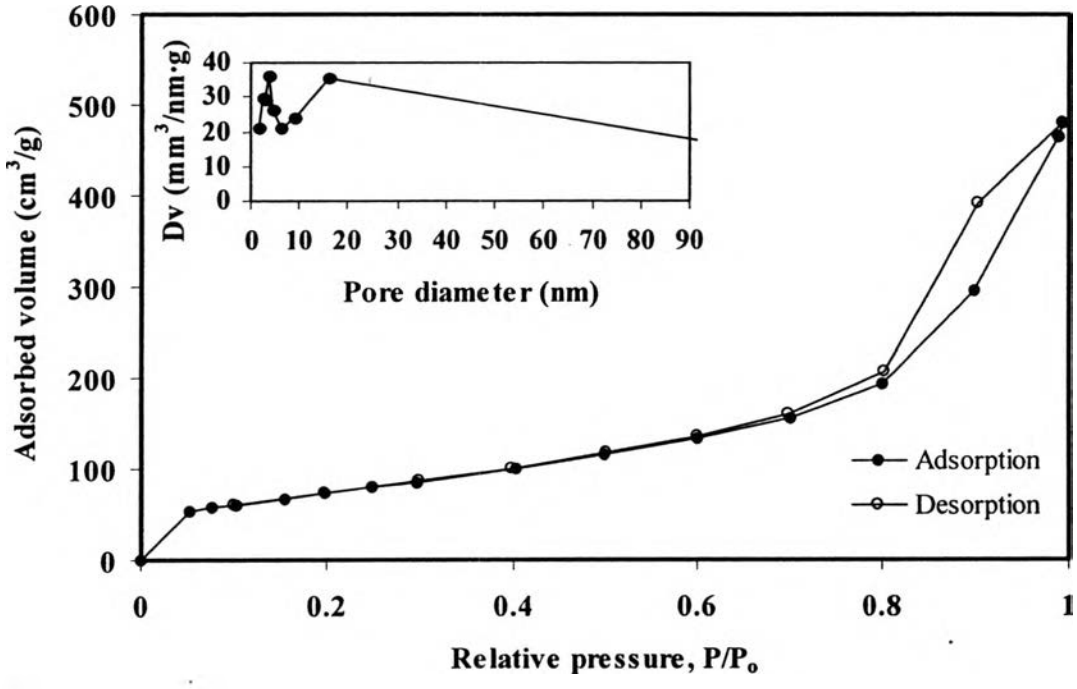

Figure 4.5 N_2 adsorption-desorption isotherms of the commercial ST-01 TiO_2 (Inset: pore size distribution).

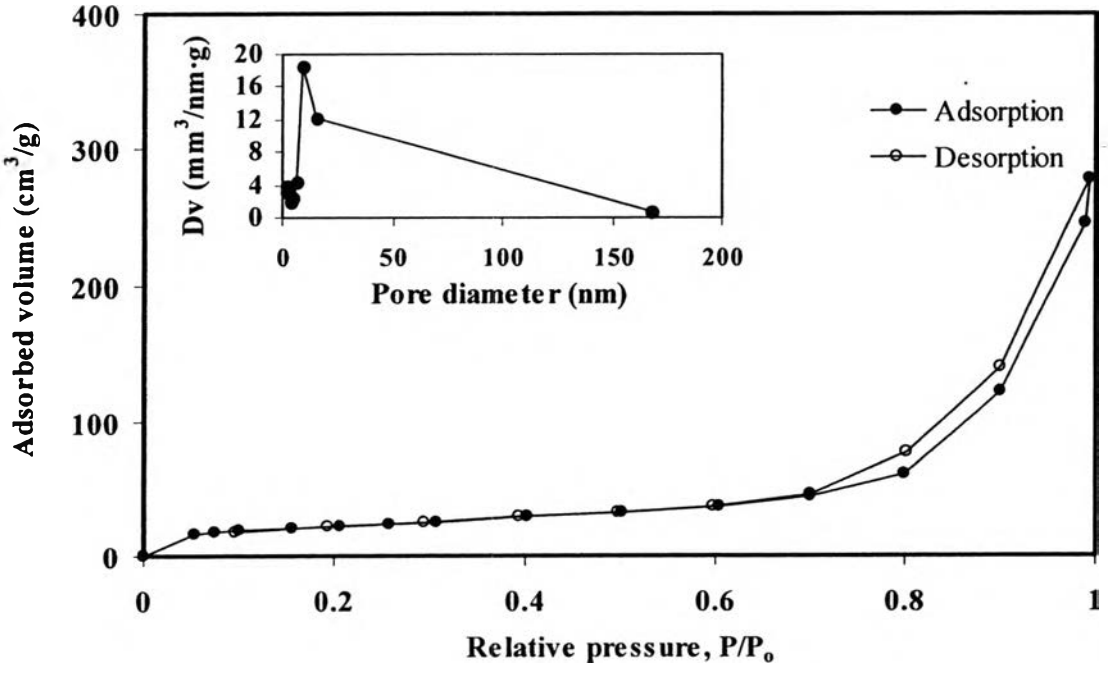

Figure 4.6 N_2 adsorption-desorption isotherms of the commercial JRC-01 TiO_2 (Inset: pore size distribution).

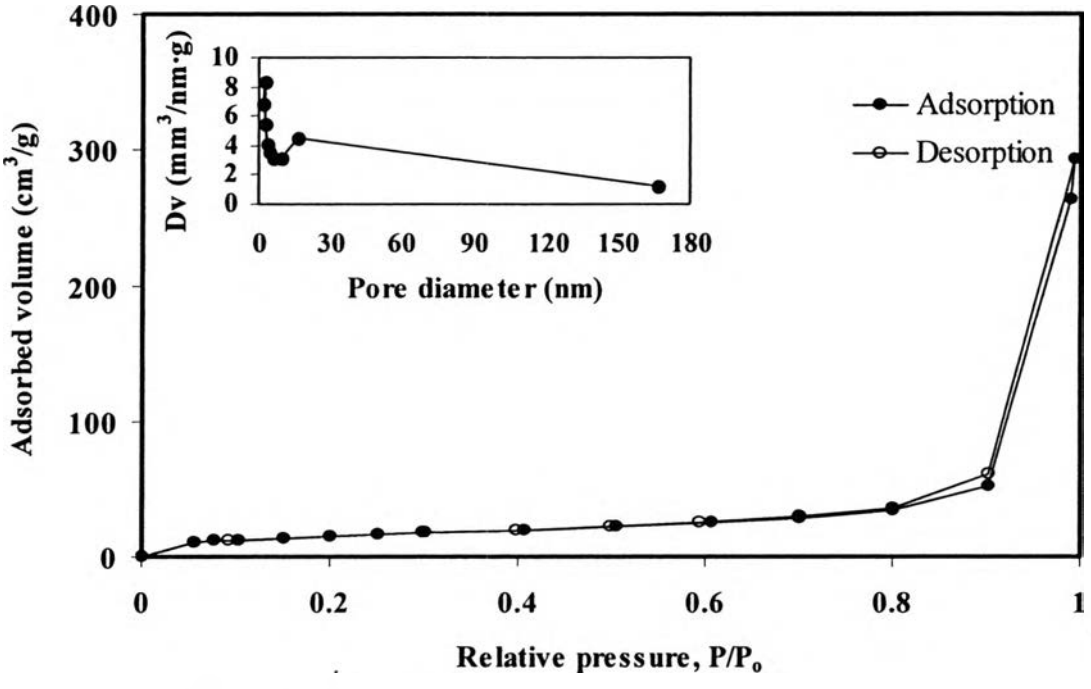

Figure 4.7 N_2 adsorption-desorption isotherms of the commercial JRC-03 TiO_2 (Inset: pore size distribution).

The textural properties obtained from N_2 adsorption-desorption isotherms, i.e. BET surface area, mean pore diameter, and total pore volume, are summarized in Table 4.2. As obviously seen, the surface area of the unloaded mesoporous-assembled TiO_2 decreased from 83.13 to 1.74 $m^2 \cdot g^{-1}$ with increasing calcination temperature from 500 to 700°C. With increasing the calcination temperature, the perceived loss in surface area is explainable to pore coalescence due to the crystallization of walls seperating mesopores. Moreover, the sintering and phase transformation of anatase to rutile phase are concerned (Lin *et al.*, 2007). Subsequently, this tendency caused an increase in mean pore diameter and a decrease in total pore volume of the bulk materials, as expected. However, the surface area of the 0.6 wt.% Pt-loaded TiO_2 is higher than that of pure TiO_2 at calcination temperature of 500°C. Plausibly, the loaded platinum could stabilize the TiO_2 framework to a certain degree and increase the surface area due to its high dispersion on TiO_2 surface. For the commercial TiO_2 photocatalysts, only BET surface area is normally reported since their N_2 adsorption-desorption isotherms correspond to

IUPAC type II pattern. The surface areas of P-25 TiO_2 and JRC-03 TiO_2 are lower than that of the mesoporous-assembled TiO_2 photocatalyst calcined at 500°C for 4 h, whereas the surface area of JRC-01 TO_2 is comparable to that of the mesoporous-assembled TiO_2. However, the surface area of ST-01 TiO_2 is much higher than those photocatalysts due to its specific production procedure.

Table 4.2 Summary of N_2 adsorption-desorption results of the synthesized mesoporous-assembled TiO_2, 0.6 wt.% Pt-loaded mesoporous-assembled TiO_2, P-25 TiO_2, ST-01 TiO_2, JRC-01 TiO_2, and JRC-03 TiO_2

Photocatalyst	Calcination temperature (°C)	Calcination time (h)	BET surface area ($m^2 \cdot g^{-1}$)	Mean pore diameter (nm)	Total pore volume ($cm^3 \cdot g^{-1}$)
Mesoporous-assembled TiO_2	500	4	83.1	6.16	0.157
	600	4	22.7	8.82	0.053
	700	4	1.7	-[a]	-[a]
0.6 wt.% Pt-loaded mesoporous-assembled TiO_2	500	4	93.8	6.18	0.153
P-25 TiO_2	-	-	65.0	-[a]	-[a]
ST-01 TiO_2	-	-	289.5	-[a]	-[a]
JRC-01 TiO_2	-	-	84.1	-[a]	-[a]
JRC-03 TiO_2	-	-	55.0	-[a]	-[a]

[a] N_2 adsorption-desorption isotherms correspond to IUPAC type II pattern.

4.1.3 XRD Results

XRD patterns of all TiO_2 photocatalysts (mesoporous-assembled TiO_2 calcined at 500-700°C, 0.6 wt.% Pt-loaded mesoporous-assembled TiO_2 calcined at 500°C, and all commercial TiO_2 photocatalysts) are shown in Figure 4.8. The phase identification and the crystallite size of the synthesized samples estimated from line broadening of anatase (101) and rutile (110) diffraction peaks using Sherrer equation (Cullity, 1978) are summarized in Table 4.3. The XRD pattern of the pure TiO_2 calcined at 500°C for 4 h shows the crystalline structure of pure anatase phase. The dominant peaks at 2θ of about 25.2, 37.9, 48.3, 53.8, 62.7, 68.9, and 75.3°, which represent the indices of (101), (103), (200), (105), (213), (116), and (107) planes, respectively, are conformed to the crystalline structure of pure anatase phase. However, at the calcination temperature of 500°C, the crystallization to anatase phase of the synthesized photocatalyst is not fully developed in comparison with the calcination temperature of 600°C, of which the peak intensity of anatase phase greatly increases. The calcination temperature of 600°C is not only determined as the highest limit for yielding well-crystalline pure anatase phase but also as the starting point of phase transformation from anatase to rutile phase since approximately 5% rutile content was observed. All calculated values of rutile ratio (W_R) in terms of weight fraction are presented in Table 4.3. The rutile ratio is estimated from XRD intensity data by using Eq. (4.1) and (4.2) (Spurr and Myers, 1957).

$$W_R = [1 + 0.8I_A/I_R]^{-1} \quad (4.1)$$

$$W_A = 1 - W_R \quad (4.2)$$

where I_A and I_R represent integrated intensities of anatase (101) and rutile (110) diffraction peaks, respectively. At the calcination temperature of 700°C, partial phase transformation from anatase to rutile was observed, resulting in combination between anatase and rutile phases with approximately 79% rutile content. The occurrence of the dominant peaks at 2θ of about 27.5, 36.0, 41.2, 44.1, 54.2, 56.7, 64.2, and 69.0°, which correspond to the indices of (110), (101), (111), (210), (211), (220), (310), and (301) planes, respectively, indicates that the rutile phase becomes the main phase in

the TiO_2 photocatalyst calcined at this temperature. For the 0.6 wt.% Pt-loaded TiO_2, the dominant peak of Pt at 2θ of about 39.7° could not be observed, presumably due to the combination of its low content, high dispersion degree, and small particle size. The results also reveal that with increasing calcination temperature, the larger TiO_2 crystallite size was obtained. However, when 0.6 wt.% Pt was loaded on the mesoporous-assembled TiO_2, smaller anatase crystallite size was observed as compared with that of the unloaded TiO_2. This might confirm the role of Pt in stabilizing the TiO_2 framework from coalescence upon calcination, leading to the obtained higher surface area (Table 4.2). In addition, the phase identification and crystallite size of all commercial TiO_2 photocatalysts are also shown in Table 4.3. The commercial P-25 TiO_2 shows the combined crystalline structure between anatase and rutile phases with approximately 26% rutile content. Unlike, the commercial ST-01 TiO_2 and JRC-01 TiO_2 show only the crystalline structure of pure anatase phase, and the commercial JRC-03 TiO_2 shows only the crystalline structure of pure rutile phase.

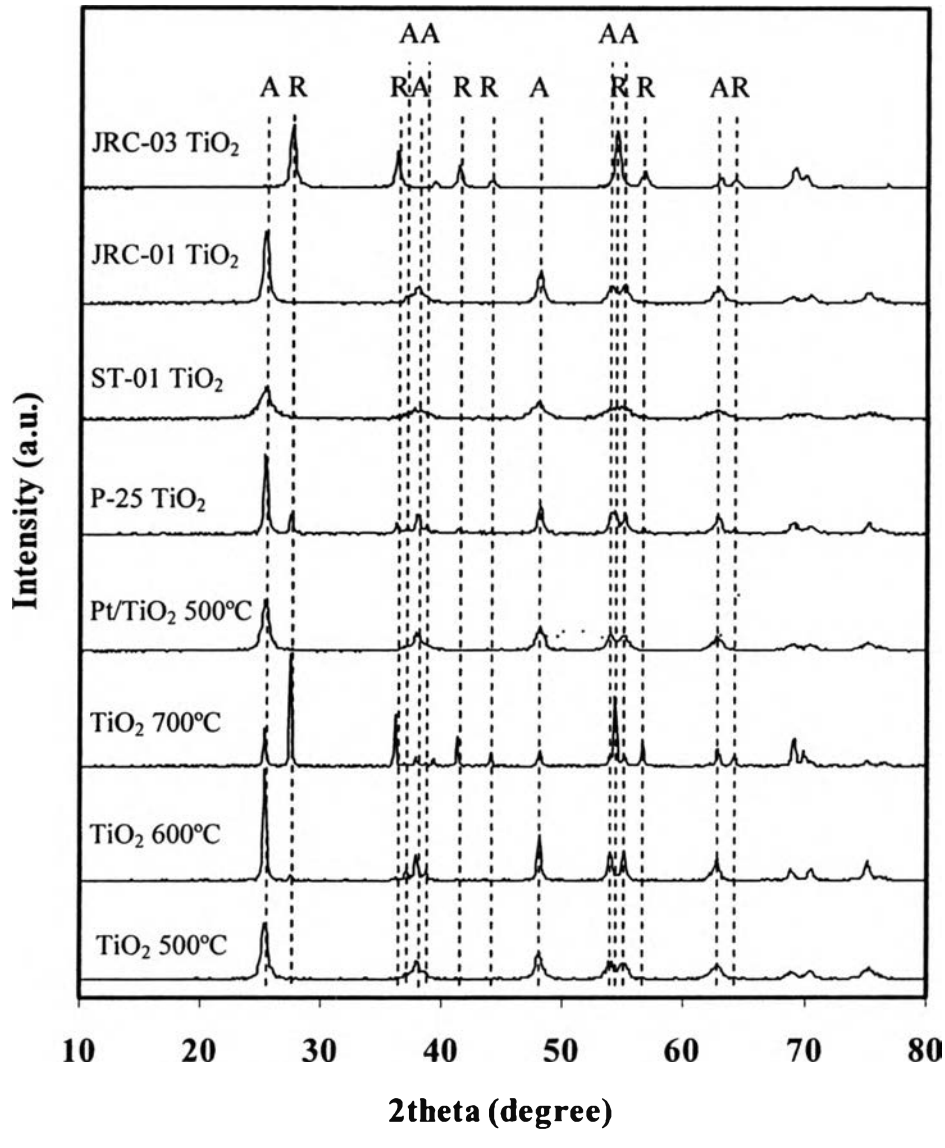

Figure 4.8 XRD patterns of the synthesized mesoporous-assembled TiO_2 calcined at 500-700°C, 0.6 wt.% Pt-loaded mesoporous-assembled TiO_2, and commercial TiO_2. (A: Anatase, R: Rutile).

Table 4.3 Summary of XRD analysis of the synthesized mesoporous-assembled TiO_2, 0.6 wt.% Pt-loaded mesoporous-assembled TiO_2, and commercial TiO_2

Photocatalyst	Calcination temperature (°C)	Calcination time (h)	Phase from XRD pattern	Rutile ratio, W_R	Crystallite size (nm)	
					Anatase (101)	Rutile (110)
Mesoporous-assembled TiO_2	500	4	Anatase	-	13.6	-
	600	4	Anatase + Rutile	0.05	25.8	46.3
	700	4	Anatase + Rutile	0.79	38.8	54.0
0.6 wt.% Pt-loaded mesoporous-assembled TiO_2	500	4	Anatase	-	12.2	-
P-25 TiO_2	-	-	Anatase + Rutile	0.26	22.0	28.9
ST-01 TiO_2	-	-	Anatase	-	8.3	-
JRC-01 TiO_2	-	-	Anatase	-	15.3	-
JRC-03 TiO_2	-	-	Rutile	1.00	-	17.1

4.1.4 UV-Vis Spectroscopy

UV-vis spectroscopy was used to examine the light absorption ability of the synthesized mesoporous-assembled TiO_2, 0.6 wt.% Pt-loaded mesoporous-assembled TiO_2, and all commercial photocatalysts (P-25 TiO_2, ST-01 TiO_2, JRC-01 TiO_2, and JRC-03 TiO_2), as well as that of Eosin Y (E.Y.) solution. The UV-Vis

spectra of the mesoporous-assembled TiO_2 calcined at 500-700°C and 0.6 wt.% Pt-loaded mesoporous-assembled TiO_2 are shown in Figure 4.9. For all commercial photocatalysts, the UV-Vis spectra are shown in the Appendix section. The results of onset absorption wavelength and corresponding band gap energy of all TiO_2 photocatalysts obtained from the UV-vis spectra are summarized in Table 4.4. It is clearly seen that the absorption band of the synthesized mesoporous-assembled TiO_2 are in the UV light range of 200-400 nm, and the shift of the onset absorption edges toward longer wavelength with the increase in calcination temperature from 500 to 700°C can be observed. This shift towards longer wavelength is normally originated from the band gap energy narrowing, consequently resulting in lower energy required for the excitation of electron from valence band to conduction band. The band gap energy (E_g, eV) is determined by extrapolating the onset of the rising part to x-axis (λ_g, nm) of the plots, as shown by dotted line in Figure 4.9, and calculated by Eq. (4.3).

$$E_g = 1240 / \lambda_g \tag{4.3}$$

where λ_g is the wavelength (nm) of the exciting light. The band gap energy of the mesoporous-assembled TiO_2 calcined at 500 and 600°C is approximately 3.2 eV ($\lambda_g \sim$ 385 and 390 nm, respectively). The results exactly conform to the band gap energy of anatase TiO_2 and therefore agree well with the results from XRD analysis. For the 0.6 wt.% Pt-loaded mesoporous-assembled TiO_2, the onset absorption wavelength was almost the same as that of the mesoporous-assembled TiO_2 calcined at 500°C, also indicating its pure anatase phase. However, the band gap energy of the mesoporous-assembled TiO_2 calcined at 700°C is approximately 3.0 eV ($\lambda_g \sim 410$ nm), which well corresponds to the band gap energy of rutile TiO_2, as also observed from the XRD analysis. Obviously, it can be noticed from the light absorption ability of all investigated TiO_2 photocatalysts that they could absorb only UV light of wavelength shorter than 420 nm. Therefore, in order to confirm that Eosin Y (E.Y.) is the visible-light responding sensitizer, its UV-vis spectrum was also measured, as shown in Figure 4.10. It is clear that E.Y. could mainly absorb the visible light with the maximum absorption centered at 516 nm. This absorption feature strongly

suggests that the sensitizer can be activated by visible light for the sensitized photocatalytic system in this study.

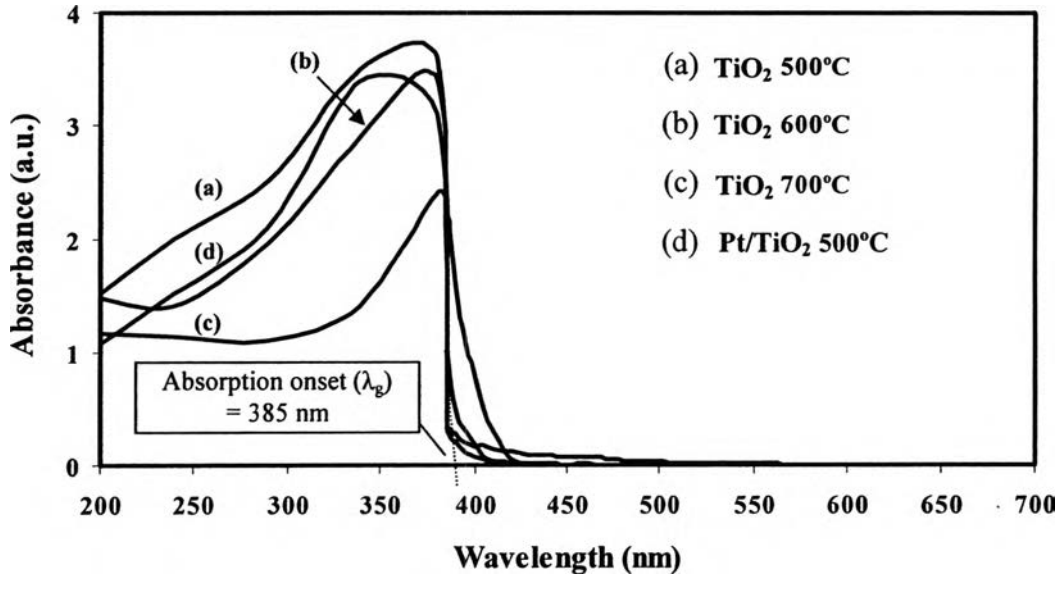

Figure 4.9 UV-Vis spectra of (a)-(c) mesoporous-assembled TiO_2 calcined at 500-700°C and (d) 0.6 wt.% Pt-loaded mesoporous-assembled TiO_2 calcined at 500 °C.

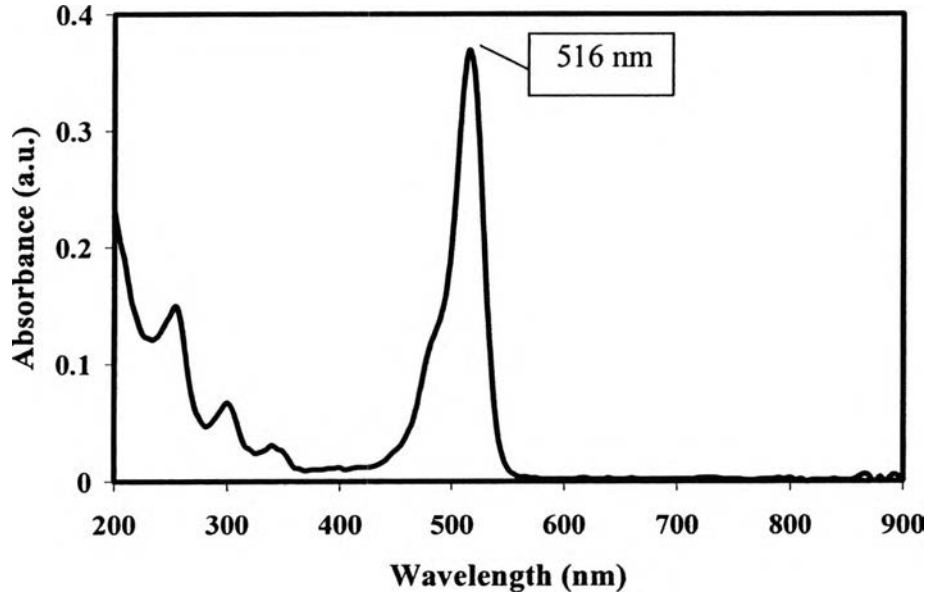

Figure 4.10 UV-Vis spectrum of Eosin Y solution.

Table 4.4 Summary of onset absorption wavelength and band gap energy of synthesized nanocrystalline mesoporous-assembled TiO_2 without and with Pt loading and commercial TiO_2 photocatalysts

Photocatalyst	Calcination temperature (°C)	Calcination time (h)	Onset absorption wavelength, λ_g (nm)	Band gap energy (eV)
Mesoporous-assembled TiO_2	500	4	385	3.22
	600	4	390	3.18
	700	4	410	3.02
0.6 wt.% Pt-loaded mesoporous-assembled TiO_2	500	4	390	3.18
P-25 TiO_2	-	-	390	3.18
ST-01 TiO_2	-	-	385	3.22
JRC-01 TiO_2	-	-	380	3.26
JRC-03 TiO_2	-	-	405	3.06

4.1.5 SEM Results

The information about the surface morphology of all synthesized TiO_2 and commercial TiO_2 was investigated by SEM. Figure 4.11 shows SEM images of all investigated TiO_2 photocatalysts. For all synthesized TiO_2, the particles with quite uniform size can be observed in form of aggregated clusters containing many nanoparticles. The aggregation plausibly leads to the formation of mesoporous-assembled structure in the synthesized photocatalysts. On the contrary, more segregated particles and less packed clusters can be observed for all commercial TiO_2. The less degree of aggregation might result in the observation of some significant extent of macroporous structure. The elemental distribution on the 0.6 wt.% Pt-loaded TiO_2 calcined at 500°C is also observed by using energy-dispersive X-ray (EDX) analysis, as shown in Figure 4.12 by elemental area mappings of each component accompanied with its SEM image. The EDX mappings show that all

elements in the Pt-loaded TiO_2 were well dispersed throughout the bulk photocatalyst due to the existence of dots in the elemental mapping of all investigated (Ti, O, and Pt) species, especially the Pt species. This is another good evidence of the high dispersion state of the deposited Pt particles.

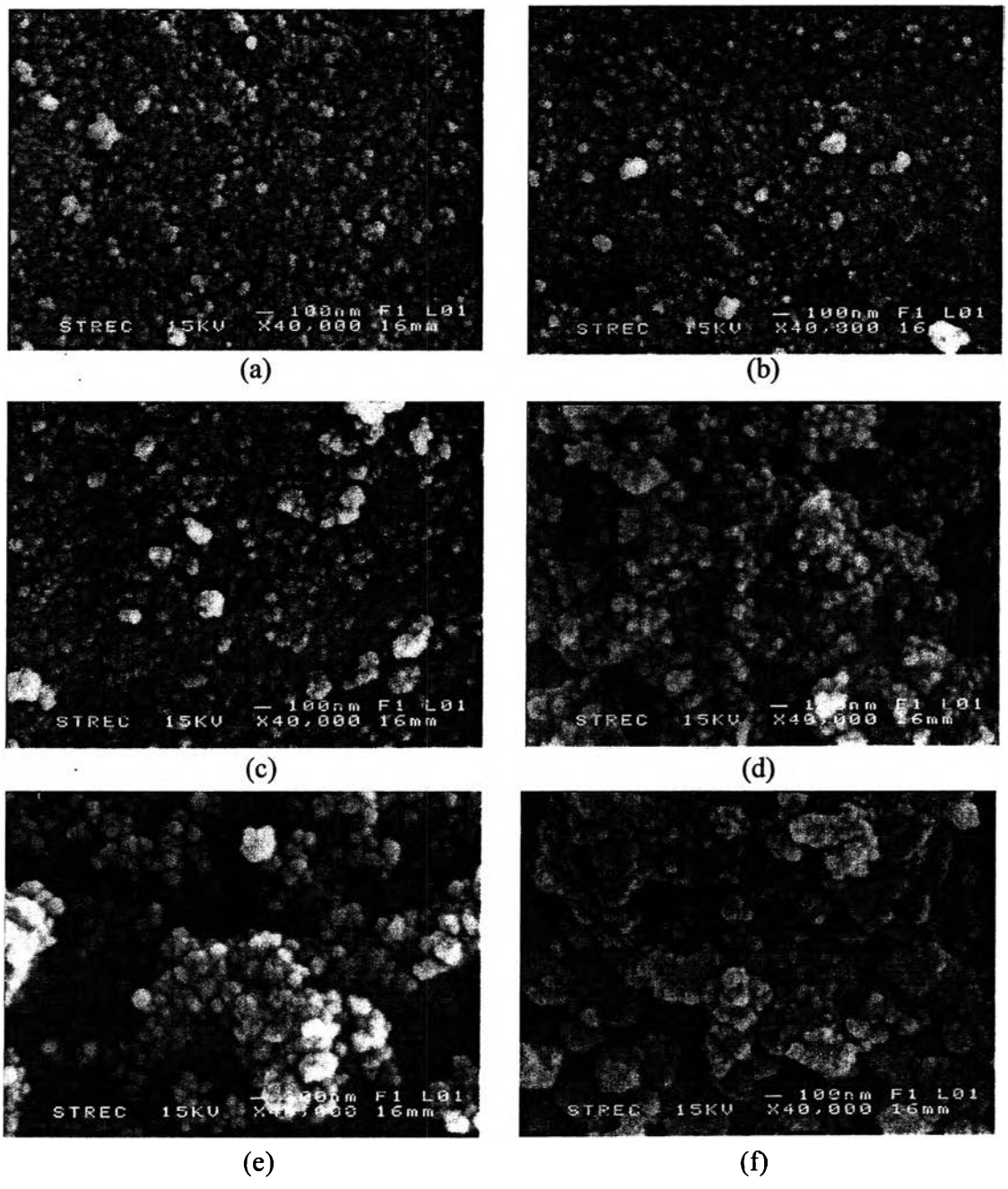

Figure 4.11 SEM images of (a) synthesized TiO_2 calcined at 500°C, (b) synthesized TiO_2 calcined at 600°C, (c) synthesized TiO_2 calcined at 700°C, (d) P-25 TiO_2, (e) ST-01 TiO_2, (f) JRC-01 TiO_2, and (g) JRC-03 TiO_2.

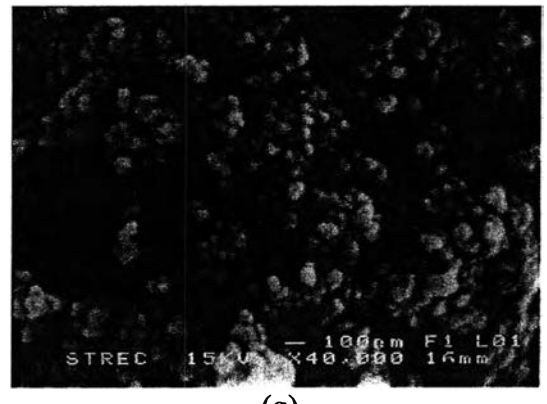

(g)

Figure 4.11 (Continued) SEM images of (a) synthesized TiO_2 calcined at 500°C, (b) synthesized TiO_2 calcined at 600°C, (c) synthesized TiO_2 calcined at 700°C, (d) P-25 TiO_2, (e) ST-01 TiO_2, (f) JRC-01 TiO_2, and (g) JRC-03 TiO_2.

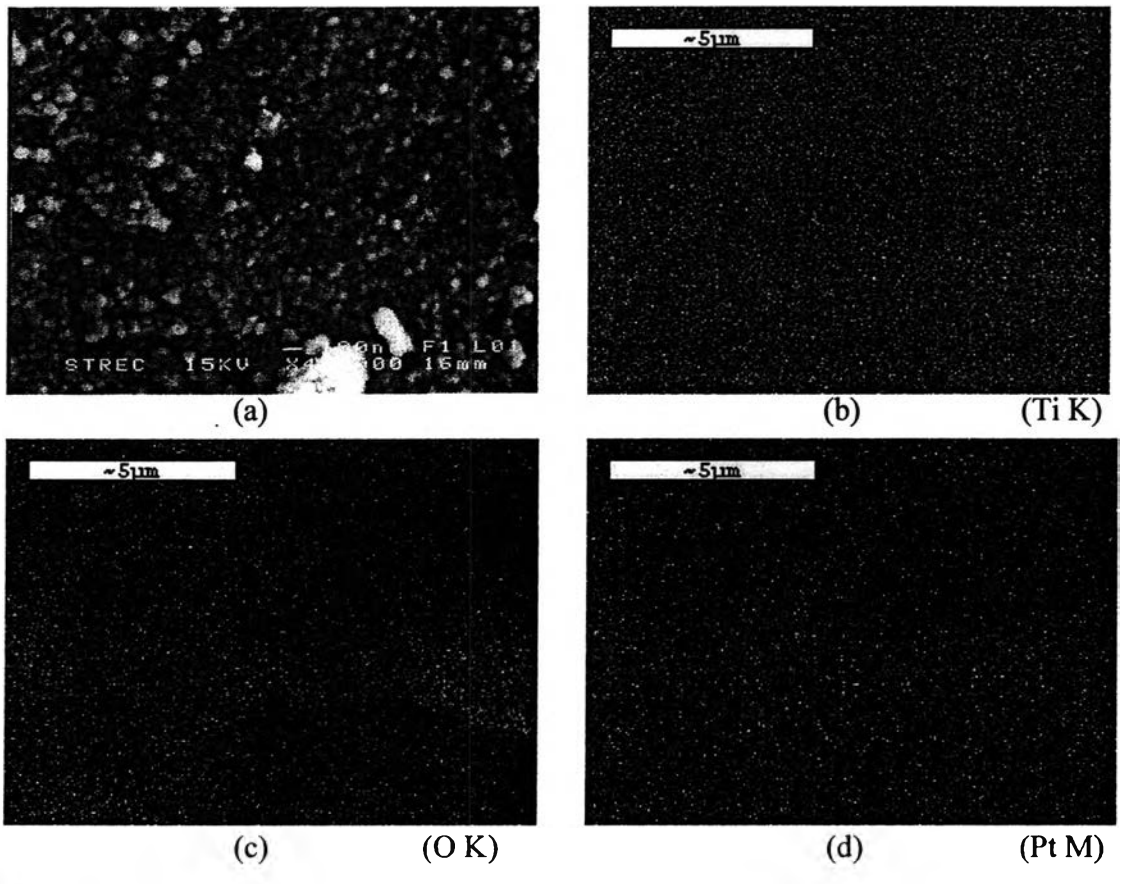

(a) (b) (Ti K)

(c) (O K) (d) (Pt M)

Figure 4.12 SEM image of 0.6 wt.% Pt-loaded mesoporous-assembled TiO_2 calcined at 500°C and EDX elemental area mappings.

4.1.6 TEM Results

In order to obtain insight information about the particle sizes of Pt and TiO_2 nanoparticles, TEM analysis was performed. The high resolution TEM (HRTEM), EDX mappings, and selected-area electron diffraction (SAED) of the 0.6 wt.% Pt-loaded mesoporous-assembled TiO_2 are shown in Figure 4.13. The HRTEM image of the sample obviously verifies that highly crystalline TiO_2 was formed due to the presence of apparent lattice fringes. The Pt phase is clearly seen as a dark patch, indicating high electron density, as confirmed by EDX mapping. The particle sizes of Pt and TiO_2 from the TEM analysis are in the range of 5-8 and 10-15 nm, respectively. The observed particle size of TiO_2 is in good accordance with the crystallite size calculated from the XRD result (13.64 nm), signifying that each grain can be considered as a single crystal. From the SAED pattern presented in the inset of the HRTEM image, all of electron diffraction rings can be indexed to the anatase phase TiO_2, which also agree well with XRD analysis. In consequence of N_2 adsorption-desorption, SEM, and TEM results, the mesoporous structure of the synthesized TiO_2 nanocrystal can be plausibly originated from the pore formed between nanocrystalline TiO_2 particles due to their aggregated assembly.

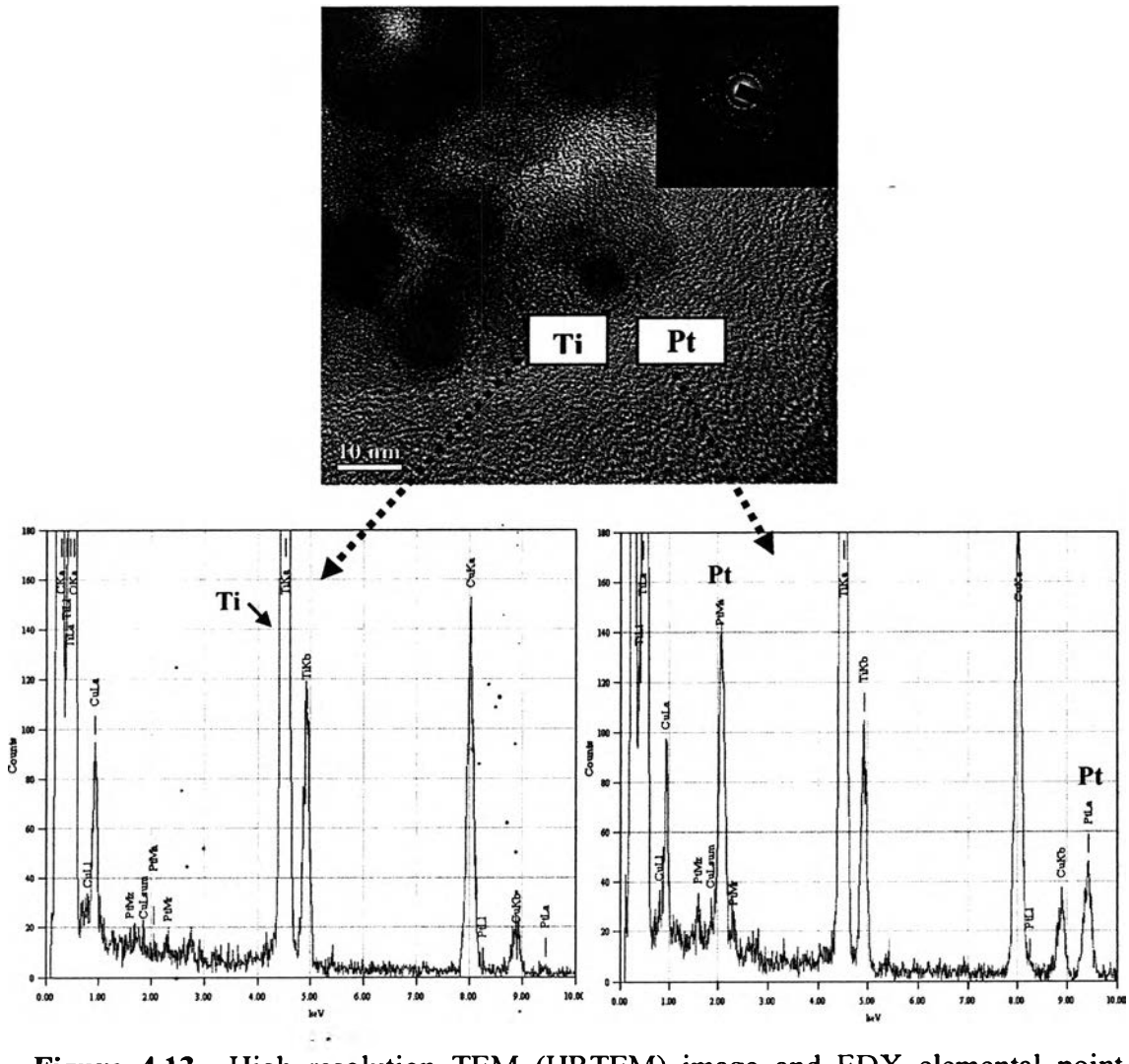

Figure 4.13 High resolution TEM (HRTEM) image and EDX elemental point mappings of the 0.6 wt.% Pt-loaded TiO_2 calcined at 500°C. (Inset of HRTEM image: selected-area electron diffraction (SAED)).

4.2 Photocatalytic Hydrogen Production Activity

In this study, the photocatalytic activity of the as-synthesized nanocrystalline mesoporous-assembled TiO_2 calcined at various calcination temperatures (500, 600, and 700°C) without and with 0.6 wt.% Pt loading was investigated for the sensitized hydrogen production from aqueous diethanolamine solution containing Eosin Y sensitizer (E.Y.) under visible light irradiation, compared with commercial P-25 TiO_2, ST-01 TiO_2, JRC-01 TiO_2, and JRC-03 TiO_2 powders. The photocatalytic activity in the absence of either light irradiation, photocatalyst, or diethanolamine was also

comparatively studied. It was found that there is no appreciable H_2 evolution in the absence of them. This confirms that the H_2 production is generated from photocatalytic water splitting over the photocatalysts. Briefly about the mechanism of sensitized photocatalytic hydrogen production, under illumination by visible light, the sensitizer is excited into its excited state. Then, the excited sensitizer can inject electrons to the conduction band of TiO_2 photocatalyst to initiate the catalytic reaction. Finally, the excited electrons in the TiO_2 conduction band can rapidly transport to the loaded cocatalyst active sites (Pt), which are deposited on the surface of TiO_2 photocatalyst, and reduce protons in the solution to generate the hydrogen. In order to regenerate the sensitizer, the oxidized-state sensitizer can be reduced by electron donor, i.e. diethanolamine in this study, and return into the ground-state sensitizer. The yield of H_2 production greatly relies on the competition between the trapping of the excited electrons by cocatalyst active sites (Pt) followed by water reduction and the electron-excited sensitizer recombination at photocatalyst surface.

4.2.1 Effect of Photocatalyst Type

In this photocatalytic reaction, a 0.2 g of different types of TiO_2 photocatalyst was first suspended in 150 ml of 15% (v/v) of diethanolamine/water mixed solution (22.5 ml of diethanolamine (DEA) and 127.5 ml of distilled water) without and with dissolved 0.1 mM Eosin Y (E.Y.) at room temperature, and the mixture was used for the photocatalytic reaction. The photocatalytic activities of the mesoporous-assembled TiO_2 calcined at 500, 600, and 700°C for 4 h (named as TiO_2 500°C, TiO_2 600°C, and TiO_2 700°C, respectively) and 0.6 wt.% Pt-loaded mesoporous-assembled TiO_2 calcined at 500°C for 4 h (named as Pt/TiO_2 500°C) in both E.Y.-free and E.Y.-containing systems were compared with commercial TiO_2 photocatalysts in both E.Y.-free and E.Y.-containing systems under the identical reaction conditions.

The results of hydrogen production rate are shown in Figures 4.14 and 4.15. It can be clearly observed that the E.Y.-containing system provided higher photocatalytic activity for hydrogen production than the E.Y.-free system, indicating that the E.Y. sensitizer greatly involves in enhancing the photocatalytic hydrogen production performance. From Figure 4.14, it can be seen that the hydrogen

production rate of the mesoporous-assembled TiO_2 calcined at 500°C in E.Y.-containing system was much higher than those of the mesoporous-assembled TiO_2 calcined at 500°C in E.Y.-free system and all commercial TiO_2 photocatalysts in E.Y.-containing system. Also, despite large surface area of about 289.5 m^2/g of ST-01 TiO_2, the imperfect crystallization from XRD data (Figure 4.8) and the non-uniform and large pore size distribution (inset of Figure 4.5) are considered to favorably increase the probability of mutual electron-excited sensitizer recombination at the photocatalyst surface defects. In case of P-25 TiO_2, the phase combination between anatase and rutile phase (rutile ratio of 0.26, as shown in Table 4.3) might be the cause of very low photocatalytic activity. It can be implied that the presence of a greater extent of rutile phase exerts a negative effect on the photocatalytic activity. By considering the location of the conduction band level, the decrement in the photocatalytic activity can be described to a lower flat band potential of rutile existing at almost similar level to the NHE potential (H^+/H_2 level), whereas that of anatase is shifted cathodically by approximately 0.2 eV. As a result, in the case of anatase TiO_2, a driving force for water reduction is sufficiently available, while a driving force for water reduction in the case of rutile TiO_2 is very small. Moreover, the lack of mesoporous-assembled structure in these commercial TiO_2 powders (P-25 TiO_2, ST-01 TiO_2, JRC-01 TiO_2, and JRC-03 TiO_2) is also subjected to less reactant accessibility for the photocatalytic reaction. In contrast, the use of the nanocrystalline mesoporous-assembled TiO_2 with uniform pore size could decrease the number of lattice defects and then facilitate the electron transport for reacting with water molecule adsorbed at TiO_2 surface along the mesoporous-assembled structure (Sreethawong *et al.*, 2005).

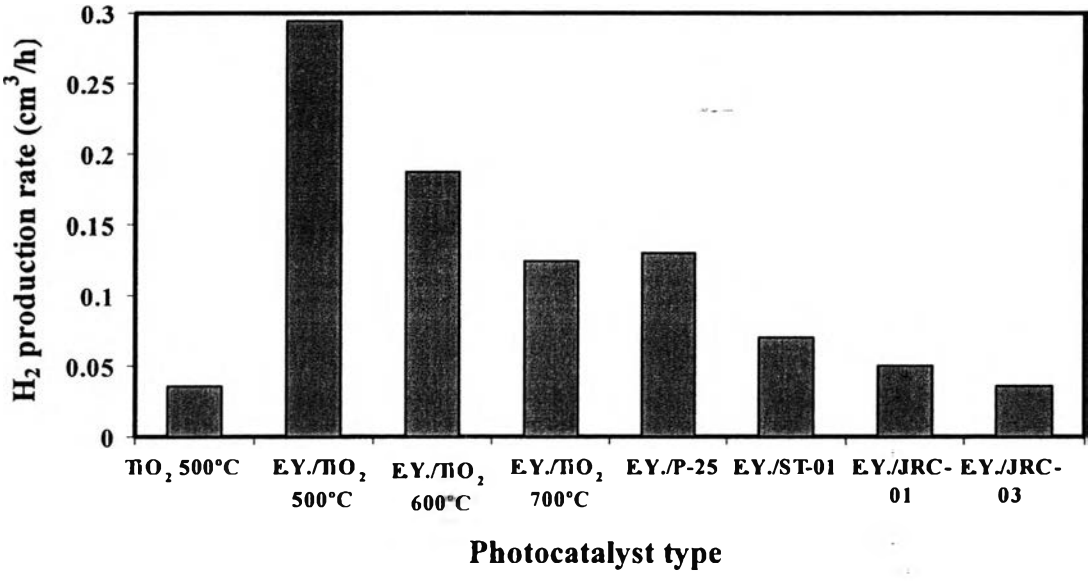

Figure 4.14 Effect of photocatalyst type on hydrogen production activity over synthesized TiO_2 photocatalyst calcined at different temperatures for 4 h in both E.Y.-free and E.Y.-containing systems compared with commercial TiO_2 photocatalysts in E.Y.-containing system (Photocatalyst, 0.2 g; total volume, 150 ml containing DEA 22.5 ml and distilled water 127.5 ml; E.Y. concentration, 0.1 mM; initial solution pH, 11.5; irradiation time, 4.h).

Besides, the presence of sensitizer in the system is very important for the photocatalytic activity because an association of the sensitizer to the photocatalyst serves as the path for electron transport from the sensitizer to the photocatalyst surface. Moreover, Pt loading has a remarkable effect on the rate of photosensitized hydrogen production, as shown in Figure 4.15. When the mesoporous-assembled TiO_2 photocatalyst without Pt loading was used for the photocatalytic reaction, the rate of sensitized photocatalytic hydrogen production was only 0.29 cm^3/h. However, when Pt nanoparticles of 0.6 wt.% loading content acting as active sites were deposited on the photocatalyst surface, the rate of sensitized photocatalytic hydrogen production was enhanced remarkably to 0.47 and 0.53 cm^3/h for the systems with Pt/TiO_2 and E.Y.-Pt/TiO_2, respectively. It can be explained in that the Pt loading can enhance both the adsorption of E.Y. sensitizer and the charge

separation of electron and excited senstitizer (Jin *et al.*, 2006). In this study, other metals, namely Ag, Ni, and Cu, of 1.5 wt.% loading content were also deposited on the mesoporous-assembled TiO_2 calcined at 500°C and used for comparative hydrogen production study. From Figure 4.15, it is clearly seen that Pt-loaded TiO_2 exhibited much superior performance in enhancing the hydrogen production activity to Ag-loaded TiO_2, whereas both Ni- and Cu-loaded TiO_2 showed unfavorably negative effect, with extremely lower photocatalytic activity than the unloaded TiO_2.

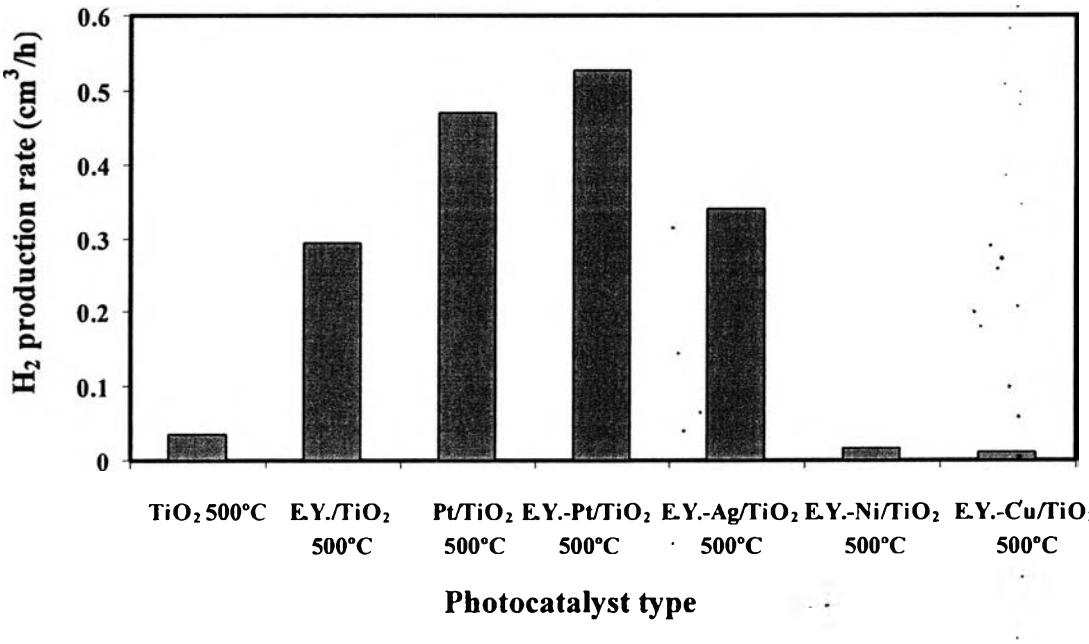

Figure 4.15 Effect of metal loading on hydrogen production activity over mesoporous-assembled TiO_2 calcined at 500°C in both E.Y.-free and E.Y.-containing systems (Photocatalyst, 0.2 g; total volume, 150 ml containing Diethanolamine 22.5 ml and distilled water 127.5 ml; Pt, Ag, Ni, and Cu loading, 0.6, 1.5, 1.5, and 1.5 wt.%, respectively; E.Y. concentration, 0.1 mM; initial solution pH, 11.5; irradiation time, 4 h).

4.2.2 Effect of Sensitizer Concentration

The concentration of E.Y. plays a significant role in the number of the electrons transferred from the excited E.Y. to TiO_2 conduction band to enhance the photocatalytic hydrogen production, as clearly seen from previous part, in which the 0.6 wt.% Pt-loaded mesoporous-assembled TiO_2 calcined at 500°C showed the

highest performance for the photocatalytic hydrogen production activity. In this part, the 0.6 wt.% Pt-loaded mesoporous-assembled TiO_2 in the E.Y.-containing system was used as the photocatalyst to investigate the effect of E.Y. concentration on the sensitized photocatalytic activity. Figure 4.16 shows the effect of dissolved E.Y. concentration (varied from 0 to 3 mM) on the photocatalytic production of hydrogen. The results show that the rate of photocatalytic hydrogen production increased with increasing the E.Y. concentration and reached a maximum at 2 mM (hydrogen production rate about 0.81 cm^3/h). However, with further increasing concentration beyond 2 mM, the hydrogen production rate decreased. To rationalize this behavior, only the fraction of the sensitizer adsorbing to the TiO_2 surface must be first recalled to be photoactive with respect to electron injection into the conduction band of the TiO_2 (Dhanalakshmi *et al.*, 2000). Initially, with the increase in the concentration of the sensitizer, such the fraction increased, hence the hydrogen production rate was significantly increased. If all the photocatalytically active sites are adsorbed by the sensitizer, there is no further increase in the hydrogen production rate with the further increase in the concentration of the sensitizer due to a saturation limit of the sensitizer adsorption sites. Thus, with further increase in the E.Y. concentration beyond the certain optimum value of 2 mM, the number of adsorbed E.Y. hardly increases. This causes the increase in the light absorption of free E.Y. in solution. Consequently, the number of the photon absorbed by E.Y. adsorbed on the surface of 0.6 wt.% Pt/TiO_2 decreases (Zhang *et al.*, 2006).

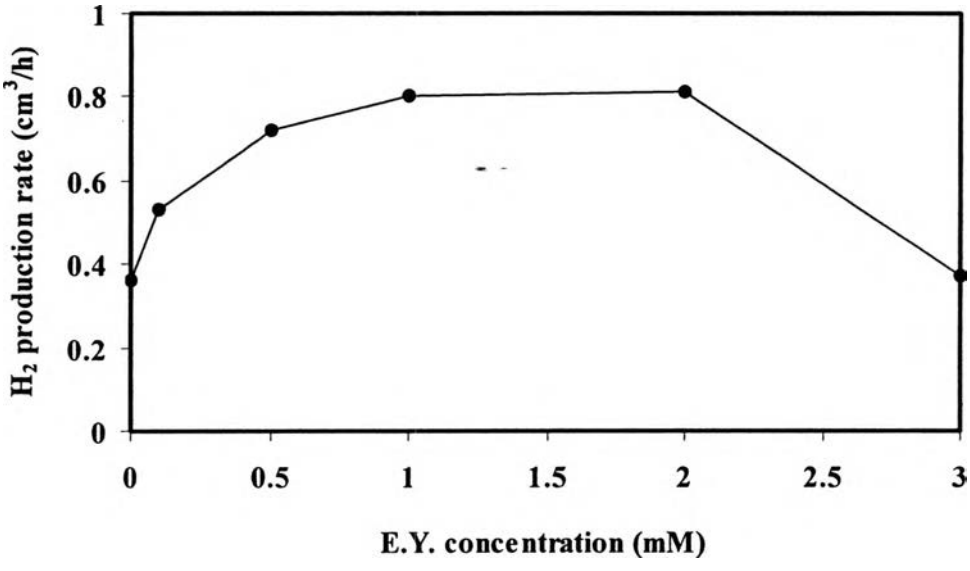

Figure 4.16 Effect of E.Y. concentration on hydrogen production activity over 0.6 wt.% Pt-loaded mesoporous-assembled TiO_2 calcined at 500°C for 4 h (Photocatalyst, 0.2 g; total volume, 150 ml containing diethanolamine 22.5 ml and distilled water 127.5 ml; Pt loading, 0.6 wt.%; initial solution pH, 11.5; irradiation time, 4 h).

In addition, as clearly observed from Figure 4.16, the sensitizer concentration of 1 mM gave just slightly lower photocatalytic activity than that of 2 mM, exhibiting the H_2 production rate of 0.80 and 0.81 cm^3/h, respectively. In order to further justify the exact optimum E.Y. concentration, the stability for photocatalytic hydrogen production over the 0.6 wt.% Pt-loaded mesoporous-assembled TiO_2 with the sensitizer concentration between 1 and 2 mM was also compared, as seen in Figure 4.17. The experimental results show that the photocatalytic activity of the E.Y.-Pt/TiO_2 at the sensitizer concentration of 2 mM was higher for long-term irradiation time, indicating the higher stability of the photocatalyst in 2 mM E.Y.-containing solution. Therefore, the sensitizer concentration of 2 mM was used for further photocatalytic activity tests.

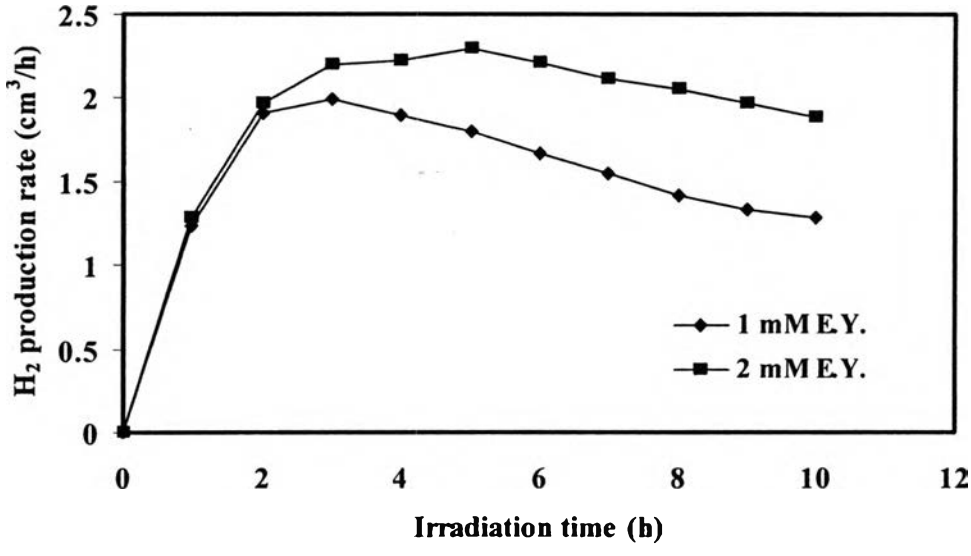

Figure 4.17 Comparison of photocatalytic activity using E.Y. concentration between 1 and 2 mM over 0.6 wt.% Pt-loaded mesoporous-assembled TiO_2 calcined at 500°C for 4 h (Photocatalyst, 0.5 g; total volume, 150 ml containing diethanolamine 22.5 ml and distilled water 127.5 ml; Pt loading, 0.6 wt.%; initial solution pH at E.Y. concentration of 1 and 2 mM, 11.3 and 11.2, respectively; irradiation time, 10 h).

4.2.3 Effect of Electron Donor Concentration

In the photosensitized hydrogen production system, the electron donor or sacrificial reagent, which was diethanolamine (DEA) in this study, could play an important role in regenerating the electron-deficient sensitizer (oxidized sensitizer). In order to obtain higher photosensitized efficiency in converting absorbed light into hydrogen energy, fast electron injection and slow backward reaction are required. The function of DEA in the present photosensitized hydrogen production process could be demonstrated in the following two reasons. First, DEA could quench the excited sensitizer species to the ground state by means of reacting with the oxidized sensitizer species. And, another reason is that it could enhance the stability of the photosensitized system for sustaining long term of hydrogen production time (Zhang *et al.*, 2007). Thus, the effect of DEA working as sensitizer regenerator needs to be studied. Figure 4.18 shows the photocatalytic hydrogen production activity of the synthesized nanocrystalline 0.6 wt.% Pt-loaded mesoporous-assembled TiO_2 photocatalyst using various DEA concentrations. The

results show that no hydrogen production was observed under visible light irradiation from the 2 mM E.Y.-containing system without dissolved DEA. Moreover, when the DEA concentration was increased, the photocatalytic hydrogen production increased, until reaching the maximum at 30 vol.% DEA (hydrogen production rate about 1.38 cm^3/h) and then levelling off. Hence, 30 vol.% DEA is the optimum concentration for effective hydrogen production. When further increasing the DEA concentration beyond the optimum level, the hydrogen production was not increased. This is probably because the DEA concentration of 30 vol.% was effectively sufficient for regenerating or quenching excited sensitizer and also preventing the electron-excited sensitizer recombination. Therefore, excess DEA in the system is not required. Since 30 vol.% DEA was experimentally verified to be the most suitable electron donor concentration for the investigated system, it was used as the main studied electron donor concentration in further experiments.

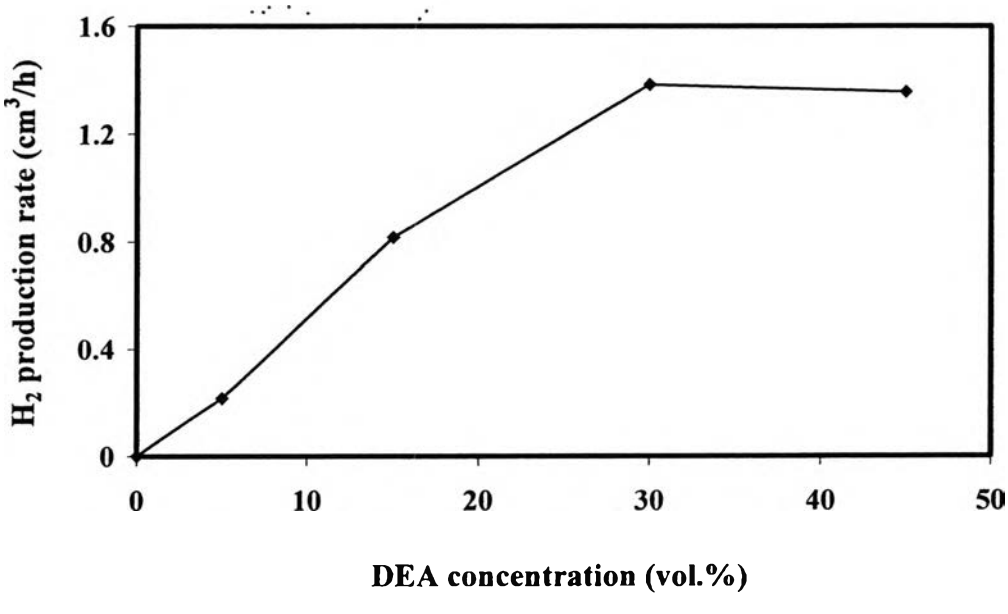

Figure 4.18 Effect of DEA concentration on hydrogen production activity over 0.6 wt.% Pt-loaded mesoporous-assembled TiO_2 calcined at 500°C for 4 h (Photocatalyst, 0.2 g; total volume, 150 ml containing diethanolamine and distilled water; Pt loading, 0.6 wt.%; initial solution pH, 11.0-11.6; irradiation time, 4 h).

4.2.4 Effect of Photocatalyst Dosage

The effect of the dosage of the synthesized nanocrystalline 0.6 wt.% Pt-loaded mesoporous-assembled TiO_2 photocatalyst in the 30 vol.% DEA/distilled water mixture solution containing dissolved 2 mM E.Y. on the photocatalytic hydrogen production was investigated. In this study, the photocatalyst dosage was varied in the range of 0-8 $g \cdot l^{-1}$ by adjusting amount of photocatalyst added into the reactor under the identical solution conditions. Figure 4.19 shows the effect of the photocatalyst dosage on the rate of hydrogen production. The results show that the photocatalyst dosage of 6 $g \cdot l^{-1}$ provided the maximum hydrogen production. Below or above this dosage, a decrease in the rate of hydrogen production was observed. A higher dosage of the photocatalyst is expected to correspond to a greater absorption of visible light energy, leading to a higher photocatalytic hydrogen production activity. However, the photocatalytic activity started to decline when the dosage of the photocatalyst exceeded the optimum value, indicating that the added amount of the photocatalyst has to be optimized. The results can be explained in the terms of availability of the active sites on the photocatalyst surface and the light penetration of the photoactivating light into the suspension (Konstantinou and Albanis, 2004). As the photocatalyst concentration increased, the availability of active sites also increased, but the light penetration and the subsequent photoactivated volume of the suspension decreased. The irradiated light could not penetrate throughout the reactor because of the covering by the large quantity of the photocatalyst in the aqueous solution. The large crowd of photocatalyst shielded the further penetration of light into the center the reactor, resulting in the block of the illuminating light. Although the light absorption of the outer photocatalyst increased, the capability of hydrogen production from the inner photocatalyst decreased due to the lack of photoexcitation. Moreover, the deactivation of active photocatalyst molecules due to the agglomeration and sedimentation of the photocatalyst particles and the consequent decrease in photocatalytic activity have also been reported (Konstantinou *et al.*, 2004). The optimum amount of the photocatalyst was required for the system in order to avoid unnecessary excess photocatalyst and also to assure total absorption of light photons for the efficient photocatalytic hydrogen production reaction. However, the photocatalyst dosage of 3.33 $g \cdot l^{-1}$ (hydrogen production rate about 2 cm^3/h) was

considered to be used in further experiments instead of the photocatalyst dosage of 6 $g \cdot l^{-1}$ (hydrogen production rate about 2.06 cm^3/h) due to the only slightly different photocatalytic activity, as well as the cost-effective concern of Pt source used at the lower photocatalyst dosage.

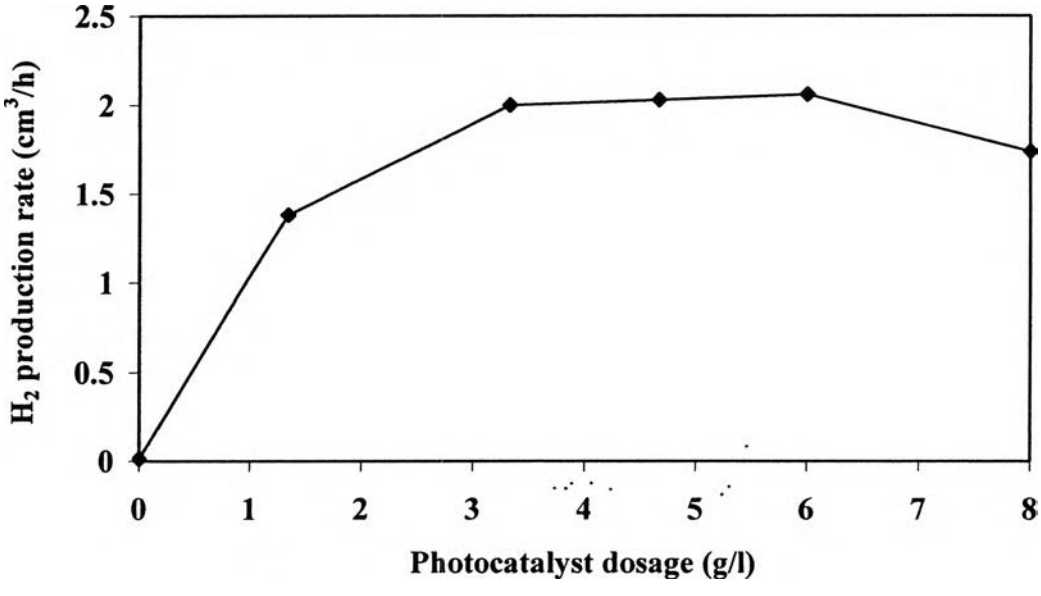

Figure 4.19 Effect of photocatalyst dosage on hydrogen production activity over 0.6 wt.% Pt-loaded mesoporous-assembled TiO_2 (total volume, 150 ml containing diethanolamine 22.5 ml and distilled water 127.5 ml; Pt loading, 0.6 wt.%; initial solution pH, 11.5; irradiation time, 4 h).

4.2.5 Effect of Initial Solution pH

One of the important parameters affecting on the photosensitized hydrogen production is the solution pH. The role of initial solution pH on the photocatalytic hydrogen production was studied in the pH range of 8.5-12.5 using DEA as an electron donor, noting that the initial pH of the original solution containing 105 ml distilled water and 45 ml DEA was approximately 11.5, and insignificant changes of solution pH were observed after the course of the photocatalytic reaction. Figure 4.20 shows the effect of the initial solution pH on the rate of hydrogen production. The experimental results indicate that the efficiency of the hydrogen production activity increased with increasing solution pH from 8.5 to 11.5, and a further increased in solution pH greater than 11.5 led to a decrease in the

hydrogen production activity. The results imply that the hydrogen production activity of the photosensitized system is favorable at nearly strong basic solution, and the optimum initial solution pH is around 11.5. A plausible explanation is that the pH value of the solution could affect the DEA oxidation reaction. It has been reported that hydrogen production increased as the solution pH increased, especially sharply at pH > 6 (Scholes *et al.*, 1967). This is because amine is more rapidly oxidized in alkaline solution since the oxidation constant of the amine is lower in an acidic solution owing to the fact that the amine is protonated. Consequently, the rate of regeneration of the sensitizer would be enhanced in alkaline solution. Therefore, the unfavorable back reaction of excited sensitizer would be retarded, and the efficiency of the utilization of excited sensitizer would be improved. Finally, the rate of hydrogen production was remarkably enhanced. However, when the initial solution pH was beyond the optimum value (too alkaline), the complexity of coulombic repulsion/interaction among OH^-, DEA, sensitizer, and photocatalyst surface might play a negative role in reducing the photocatalytic activity.

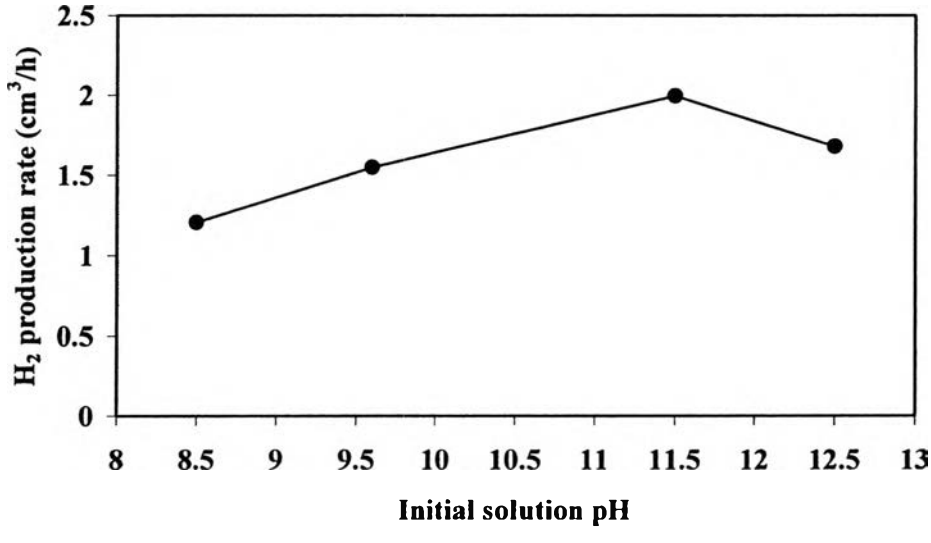

Figure 4.20 Effect of initial solution pH on hydrogen production activity over 0.6 wt.% Pt-loaded mesoporous-assembled TiO_2 calcined at 500°C for 4 h (Photocatalyst, 0.5 g; total volume 150 ml containing 45 ml diethanolamine and 105 ml distilled water; Pt loading, 0.6 wt.%; irradiation time, 4 h).